Journal of Materials Chemistry

Cite this: J. Mater. Chem., 2012, 22, 12695

www.rsc.org/materials

PAPER

A ZnO/N-doped carbon nanotube nanocomposite charge transport layer for high performance optoelectronics†

Ji Sun Park,‡[a] Ju Min Lee,[a] Sun Kak Hwang,[a] Sun Hwa Lee,[a] Hyun-Jung Lee,[b] Bo Ram Lee,[b] Hyung Il Park,[a] Ji-Seon Kim,[ac] Seunghyup Yoo,[d] Myoung Hoon Song*[b] and Sang Ouk Kim*[a]

Received 6th February 2012, Accepted 15th April 2012
DOI: 10.1039/c2jm30710c

Metal oxide charge transport layers are widely used to promote the interfacial charge transport of organic optoelectronics. Nevertheless, frequently used wide-bandgap metal oxides with low electrical conductivities reveal inherent limitations in the charge transport enhancement. We present the remarkable electro-conductivity enhancement of solution processable ZnO charge transport layers upon dispersing a tiny amount (less than 0.1 wt%) of chemically doped CNTs and the corresponding device performance improvement of light-emitting diodes (OLEDs). Using various undoped or doped CNTs, whose work function was systematically tuned by substitutional doping of electron deficient B or electron rich N,N-doped CNT (N-CNT), the composite showed a lowered work function matching well with the conduction band of ZnO. Consequently, the ZnO/N-CNT nanocomposite transport layer with 0.08 wt% N-CNT showed a five-fold enhancement of electron mobility, while maintaining the intrinsic bandgap energy levels, optical transparency and solution processability of pure ZnO. The inverted OLEDs employing ZnO/N-CNT nanocomposite electron transport layers could facilitate well-balanced electron–hole injection and, thus, more than two-fold enhancement of maximum luminance (from 21 000 cd m^{-2} at 14.6 V to 46 100 cd m^{-2} at 14.0 V) and efficiency (from 6.9 cd A^{-1} at 13.4 V to 14.3 cd A^{-1} at 13.6 V). This highly effective charge mobility enhancement enabled by work function tunable, chemically doped CNTs would be beneficial for various organic and inorganic charge transport materials with different energy levels.

Introduction

The interfacial charge transport layer is an essential device element for high performance optoelectronics.[1–3] A charge transport layer can effectively mitigate interfacial energy level mismatch to attain barrier-free charge injection and transport.[4] To date, various metals,[5] metal salts,[6] semiconducting polymers,[7] and dipolar molecules[8–14] have been exploited for the effective charge transport of organic optoelectronics. Nevertheless, corrosive metal elements, or low stability of thin organic layers inherently limits the long-term reliability of device operation. Recently, ultrathin metal oxide films of ZnO,[15–17] TiO_2,[18] ZrO_2,[19] and HfO_2[20] have emerged as promising alternatives with exceptional environmental stability, optical transparency, and mechanical robustness.[21] Moreover, the solution processability of the metal oxides is compatible with the large area printing process of organic devices. Despite such advantages, the semiconducting or even insulating metal oxides with large band gaps generally exhibit low electrical conductivity and reveal inherent limitations in charge transport enhancement while mitigating energy levels. Presently, the doping of carrier-rich elements[22,23] or photo exposure[24] is widely exploited to improve the electro-conductivity of metal oxides. Nonetheless, the high cost vacuum process, the undesired alternation of energy levels, and the radiative damage of the active layer raise formidable technological obstacles.

Graphitic carbon materials, including carbon nanotubes (CNTs) and graphene, possess outstanding carrier mobility and other desirable electrical properties that can be sustained under

[a]*Department of Materials Science and Engineering, KAIST, Daejeon, 305-701, Republic of Korea. E-mail: sangouk.kim@kaist.ac.kr; Fax: +82 42 350 3310; Tel: +82 42 350 3339*
[b]*School of Mechanical and Advanced Materials Engineering and Low Dimensional Carbon Materials Center, Ulsan National Institute of Science and Technology (UNIST), Banyeon-ri 100, Ulsan, 689-805, Republic of Korea. E-mail: mhsong@unist.ac.kr; Fax: +82 52 217 2109; Tel: +82 52 217 2316*
[c]*Department of Physics and Centre for Plastic Electronics, Imperial College London, Prince Consort Road, London, SW7 2AZ, UK*
[d]*Department of Electrical Engineering, KAIST, Daejeon, 305-701, Republic of Korea*

† Electronic supplementary information (ESI) available: XPS analysis of undoped and doped CNTs, preparation of homogeneously dispersed ZnO/CNT precursor solutions, light-emitting characteristics of OLEDs with various concentrations of N-CNTs in the ZnO layer, *J–V* characteristics of electron-only devices with various concentrations of N-CNTs in the ZnO layer, the bandgap energy of ZnO/CNT nanocomposite layers obtained from the UV-VIS absorption spectrum, the work function measurement of undoped and doped CNTs by UPS. See DOI: 10.1039/c2jm30710c

‡ Present address: Energy NanoMaterials Research Center, Korea Electronics Technology Institute (KETI), Seongnam, Republic of Korea.

a severe deformation.[25–27] Such attractive characteristics render graphitic carbon materials as valuable component materials for organic optoelectronics.[28] Nevertheless, previous research efforts for the optoelectronic application have suffered from the poor tunability of the work function (4.7–5.2 eV) caused by the use of the inert graphitic chemical structure.[29,30] A mismatched and uncontrollable work function makes it hard to engineer the interfacial energy level and to optimize charge transport in optoelectronic devices. To date, several approaches have been explored to modulate the work function of graphitic carbon materials, including the physisorption of ions,[31] molecules,[32] or nanoparticles.[33] In those approaches, however, the desorption of the physisorbed dopants may cause deterioration of device performance in long-term operations.

In this work, we demonstrate a robust pathway to enhance the electrical conductivity of solution processable metal oxide charge transport layers, while maintaining their intrinsic energy levels, by dispersing substitutionally doped CNTs. The substitutional doping of electron-deficient boron (B) or electron-rich nitrogen (N) systematically altered the work function of CNTs and endured high temperature treatment involved in the solution processing of thin ZnO/CNT nanocomposite layers *via* spray-pyrolysis.[34,35] Among various undoped or doped CNTs, N-doped CNT (N-CNT) showed a work function closely matching the conduction band of ZnO to form an ohmic contact for electron transport.[36] The resultant ZnO layer with finely dispersed, high mobility N-CNTs demonstrated remarkable enhancement of electron mobility. Unlike widely used atomic scale foreign element doping, nanocomposites employing high carrier mobility nanomaterials did not alter the intrinsic energy level of metal oxides. The ZnO/N-CNT nanocomposite layer with improved electron mobility enabled balanced electron and hole injection, and device performance optimization of inverted organic light-emitting diodes (OLEDs).

Experimental

B- and N-doping of multi-walled CNTs

Commercially available CNTs (>95%, multi-walled nanotubes) grown by chemical vapor deposition (CVD) were purchased from Hanwha Nanotech. The average diameter of CNTs was 10–15 nm. 1 g of CNTs was sonicated in 500 mL strong acid solution (3 : 1 mixture of HNO_3 and H_2SO_4) for 10 hours and then washed with deionized (DI) water and filtered for purification. After drying, the CNTs were thermally treated at 400 °C for 40 min to remove amorphous carbons. The average length of the purified CNTs was less than 1 μm. For B-doping, the purified CNTs were mixed with powdered B_2O_3 and placed in an open sintered pure graphitic crucible. The weight ratio of B_2O_3 : CNTs in the crucible was 5 : 1. The B_2O_3–CNT mixture was thermally treated at 1100 °C for 4 hours under an Ar (40 sccm)/NH_3 (60 sccm) mixture gas flow. After thermal treatment, the remaining B_2O_3 powder was washed with hot boiled DI water. For N-doping, the purified CNTs in the crucible were thermally treated at 1100 °C for 4 hours under Ar (40 sccm)/NH_3 (60 sccm) gas flow.

ZnO/CNT precursor solution preparation

The zinc acetate dihydrate (Sigma-Aldrich, 16.5 mg) was dissolved in 2-methoxyethanol (Sigma-Aldrich, 100 mL) with a stabilizer of ethanolamine (Sigma-Aldrich, 5 mL) (solution A). CNTs (10.5 mg) were subsequently dispersed in ZnO precursor solutions by ultrasonication for 4 hours. A ZnO/CNT precursor solution was maintained under ambient conditions for 24 hours, after which centrifugal separation (15 000 rpm, 30 min, Hanil Science Industrial Co., Ltd., Supra 22K) was performed to separate the homogeneously dispersed supernatant. The well-dispersed supernatant was re-dispersed in solution A without CNT, and finally, a transparent solution without any precipitate was obtained (solution B). To adjust the desired amount of CNTs within a 70 nm thick ZnO layer, the prepared solution B was added in zinc acetate dehydrate–methanol solution (8 wt%). The concentrations of CNTs within the zinc acetate dihydrate–methanol solution were 0.04, 0.08 and 0.12 wt% of zinc acetate dihydrate, respectively (solution C) (see ESI, Fig. S1†).

Inverted organic light-emitting diode fabrication

F:SnO_2 (FTO) substrates were cleaned by sequential ultrasonication in acetone and isopropyl alcohol (IPA), and dried under a stream of N_2. A 70 nm thick ZnO/CNT nanocomposite layer was deposited onto the cleaned FTO substrate by the spray-pyrolysis method. The spray pyrolysis was performed at 400 °C on a hotplate using a conventional air-sprayer. The precursor solution C was intermittently sprayed onto the substrate (spraying time: 10 s, interval time for vapouring the solvents: 20 s). The CS_2CO_3 layer was spin cast onto the ZnO/CNT nanocomposite layer from 0.5 wt% 2-methoxyethanol solution. The poly(9,9′-dioctylfluorene-*co*-benzothiadiazole) (F8BT) layer was spin cast from a *p*-xylene solution and annealed at 155 °C for 1 h under a nitrogen atmosphere. Finally, a 10 nm thick MoO_3 layer and a 60 nm thick Au layer were thermally evaporated onto the polymer surface at a slow deposition rate of 0.3 Å s^{-1}.

Characterization

A UV-VIS spectrometer (Jasco, V530) was utilized to measure the optical transmittance and the absorbance of ZnO/CNT nanocomposite layers. The surface morphology and roughness of ZnO/CNT nanocomposites were measured by scanning electron microscopy (SEM, Hitachi, S-4700) and atomic force microscopy (AFM, Seiko Instruments, Inc., SPI3800N/SPA400). The work function of ZnO/CNT nanocomposites was obtained from ultraviolet photoelectron spectroscopy (UPS, AXIS-NOVA, Kratos, Inc.). X-ray photoelectron spectroscopy (XPS) measurements were carried out with a Sigma Probe with a microfocused monochromatic X-ray source (Thermo VG Scientific, Inc.). Current density and luminance *vs.* applied voltage (*J*–*V*–*L*) characteristics were measured using a Keithley 2400 source measurement unit and a Konica Minolta spectroradiometer (CS-2000).

Results and discussion

Fig. 1(A) and (B) respectively illustrate the chemical structure of green-light-emitting F8BT and the device architecture of inverted OLEDs used in this work. The device was prepared by sequential deposition of ZnO/CNT nanocomposites (electron transporting layer), CS_2CO_3 (hole blocking layer), F8BT (light-emitting active layer), MoO_3 (hole transporting layer), and Au (anode) on

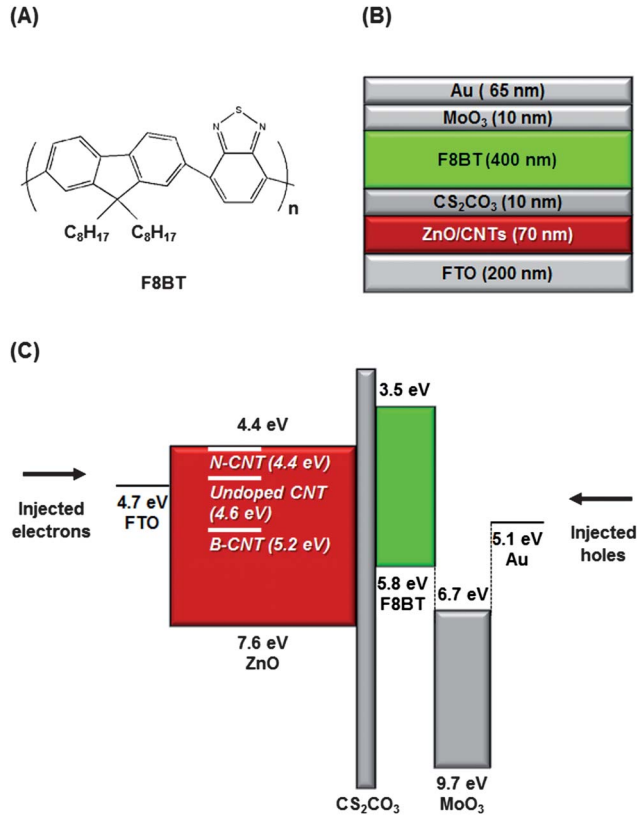

Fig. 1 (A) Chemical structure of F8BT and (B) device architecture of OLEDs with ZnO/CNTs (undoped CNT, B-CNT, or N-CNT) nanocomposite charge transport layers. (C) Energy level diagram for all the layers in the inverted organic light-emitting diodes (OLEDs).

a commercially available FTO transparent electrode/glass substrate (cathode). Fig. 1(C) shows the energy level diagram of the fabricated device. The original device architecture with a pure ZnO electron transport layer is known to exhibit hole dominant device characteristics owing to the ohmic contact at the anode mediated by the MoO_3 hole transporting layer.[37,38] Therefore, electron transport enhancement is needed at the cathode to compensate for the hole dominance and to optimize device performance.

As reported in our previous work,[36] B-doping of CNTs was performed by thermal treatment with vaporized B_2O_3 under an Ar–NH_3 gas flow mixture.[39] The NH_3 was introduced as an etching gas to induce vacancy defects with CN_x and C_xH_y groups. Further reaction with vaporized boron resulted in the substitutional B-doping of CNTs.[40] For N-doping, similar thermal treatment was performed but without B_2O_3. Quantitative doping-level measurements by XPS, elemental analysis (EA) and inductively coupled plasma-mass spectroscopy (ICP-MS) demonstrate that B-CNT was 3.0 atom% B-doped and 0.5 atom % N-doped, while N-CNT was 3.4 atom% N-doped (ESI, Fig. S2†). A 70 nm thick ZnO/CNT nanocomposite charge transport layer was deposited by spray pyrolysis (ESI, Fig. S1†). The CNT content within the ZnO layer was maintained at 0.08 wt% for maximized OLED performance. Excessive CNTs aggregated and degraded OLED performance (ESI, Fig. S3 and S4†). As shown in Fig. 2(A) and (B), the surface morphology of the prepared ZnO/CNT nanocomposite layer revealed anisotropic, elongated particles that were obviously distinct from those of the pristine ZnO layer. This morphological modification was attributed to the incorporation of long CNTs within ZnO particles. The average surface rms roughness of the ZnO and ZnO/CNT layers measured by AFM showed similar values of 6.6 nm and 8.6 nm, respectively (Fig. 2(C) and (D)). Those values were small enough to reduce the high surface roughness of the FTO electrode (13.5 nm). The UV-VIS spectrum measurements shown in Fig. 2(E) confirmed that the finely dispersed 0.08 wt% CNTs did not significantly influence the optical transmittance of the ZnO layer. The bandgap energy of ZnO/CNT nanocomposite layers also maintained the same value as that of the ZnO layer (~3.2 eV) (ESI, Fig. S5†). A 10 nm thick CS_2CO_3 layer and a 400 nm thick F8BT layer were sequentially spin cast onto the ZnO/CNT nanocomposite layer, above which a 10 nm thick MoO_3 layer and a 60 nm thick Au layer were thermally evaporated to complete the device fabrication.

For efficient electron transport within a ZnO/CNT layer, the work function of metallic CNTs should match the conduction

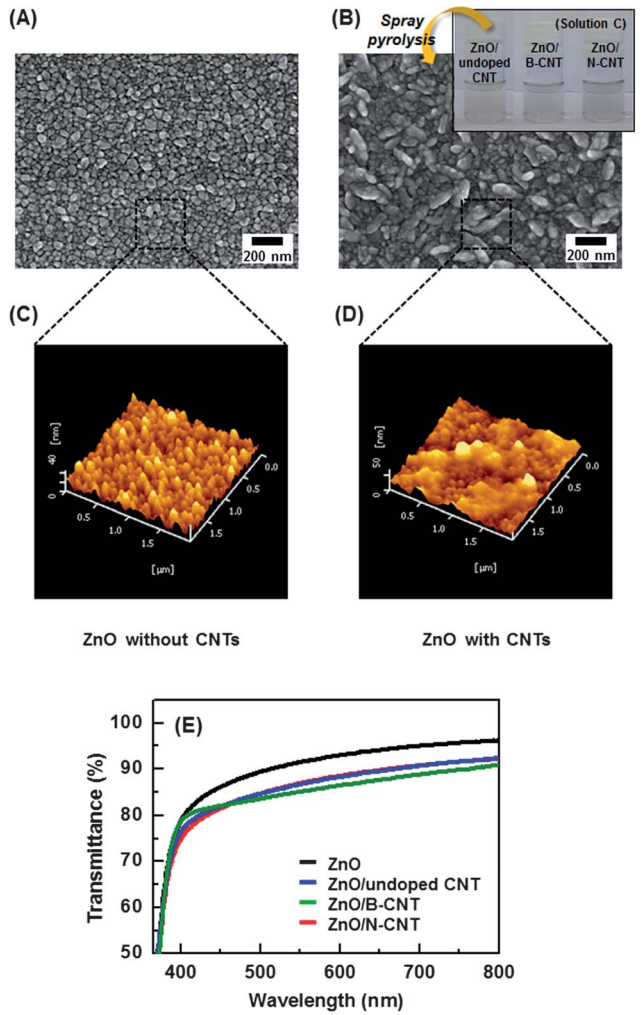

Fig. 2 SEM and AFM images of a ZnO layer (A), (C) without and (B and D) with CNTs prepared by spray-pyrolysis deposition, respectively. (E) Transmittance of ZnO/CNTs (undoped CNT, B-CNT, or N-CNT) nanocomposite layers with thickness 70 nm.

band of semiconducting ZnO (4.4 eV). The work functions of undoped and doped CNTs were compared by ultraviolet photoelectron spectroscopy (UPS) measurements (ESI, Fig. S6†).[36] While undoped CNTs showed a work function of 4.6 eV, B-CNTs showed a significantly increased value of 5.2 eV. Since B has one fewer electron than carbon, the B-doping lowered the π electron density and, thus, increased the work function. In contrast, the work function of N-CNT decreased down to 4.4 eV due to the additional π electrons from doped N atoms. As schematically illustrated in Fig. 3(A), the Fermi level of N-CNT matched well with the conduction band edge of ZnO. In this ideal ohmic contact, electrons transported freely between semiconducting ZnO and metallic N-CNTs without any barrier such that metallic CNTs of micrometre length provided high mobility pathways to promote the overall electron transport through the ZnO/CNT nanocomposite layer. Meanwhile, the Fermi level of undoped CNT or B-CNT was deeper than the conduction band edge of ZnO. While the electron transport from ZnO to CNT was barrier-free, the reversed transport from CNT to ZnO would encounter an energy barrier. The resultant electron trap in the dispersed CNTs could deteriorate the overall electron transport through the nanocomposite layer.

The electron transport *via* pure ZnO and ZnO/CNT nanocomposite layers was straightforwardly compared by the characteristics of electron-only devices described in Fig. 3(B). Due to the large energy mismatch between the work function of Al (4.3 eV) and the valence band of ZnO (7.6 eV), hole transport was effectively blocked in this architecture. The current density (*J*) *vs.* applied voltage (*V*) plots evidently demonstrated the beneficial role of CNTs and the significance of the energy level matching between the conduction band of ZnO and the work function of CNTs in enhancing electron transport. While the B-CNTs with a large energy barrier to ZnO for electron injection caused significantly deteriorated electron transport, the N-CNTs with a barrier-less, ohmic contact revealed remarkable enhancement of electron transport. In the case of undoped CNTs, which had a relatively small energy barrier of ~0.2 eV to ZnO, electron transport was still improved, but only by a small amount.

The light-emitting characteristics of the OLEDs with ZnO and nanocomposite electron transport layers are presented in Fig. 4. Fig. 4(A)–(D) present the current density and luminance *vs.* applied voltage (*J*–*V*–*L*) plots. The reference OLED without CNTs showed an EL efficiency of 6.9 cd A^{-1} (at 13.4 V) and a luminance of 21 000 cd m^{-2} (at 14.6 V), respectively (Fig. 4(A)). The device with 0.08 wt% B-CNTs exhibited degradation in EL efficiency and luminance down to 4.2 cd A^{-1} (at 14.0 V) and 10 900 cd m^{-2} (at 14.8 V), respectively (Fig. 4(C)). In contrast, the OLEDs with undoped CNTs (Fig. 4(B)) or N-CNTs (Fig. 4(D)) showed enhanced EL efficiency and luminance. The device with N-CNTs exhibited the largest (more than two-fold) enhancement, resulting in luminance of up to 14.3 cd A^{-1} (at 13.6 V) and 46 100 cd m^{-2} (at 14.0 V), respectively. Fig. 4(E) compares the device EL efficiency (η_{EL}) *vs.* luminance (*L*), and Fig. 4(F) compares the luminance *vs.* current density (*L*–*J*) plot. The electron transport enhancement by N-CNTs effectively optimized the electron–hole balance, enhancing the electron–hole recombination probability within the light-emitting F8BT layer. We note that a well-balanced carrier transport was more dominant in the high luminance range. In the low-voltage range

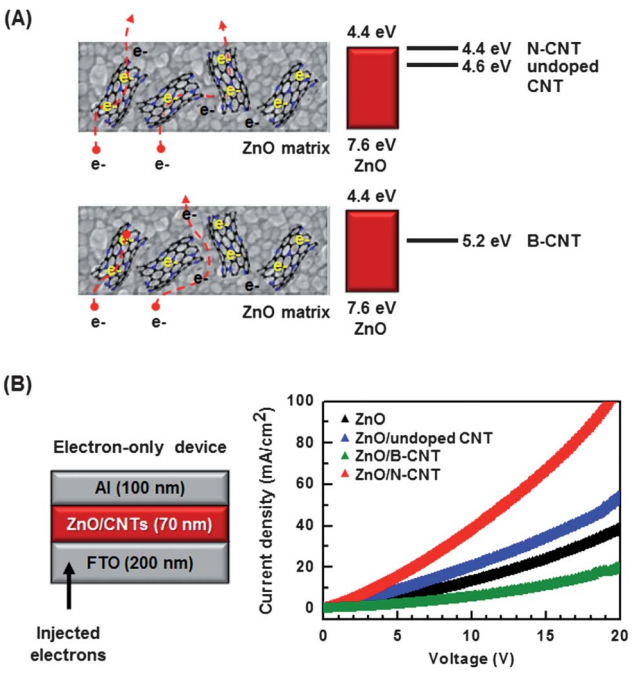

Fig. 3 (A) Schematics of the proposed mechanism for electron transport within ZnO/N-CNT, ZnO/undoped CNT and ZnO/B-CNT electron transport layers. B-CNTs trap electrons due to the high work function. (B) Electron-only device architecture and *J*–*V* plots for ZnO, ZnO/undoped CNT, ZnO/B-CNT, and ZnO/N-CNT nanocomposite layers.

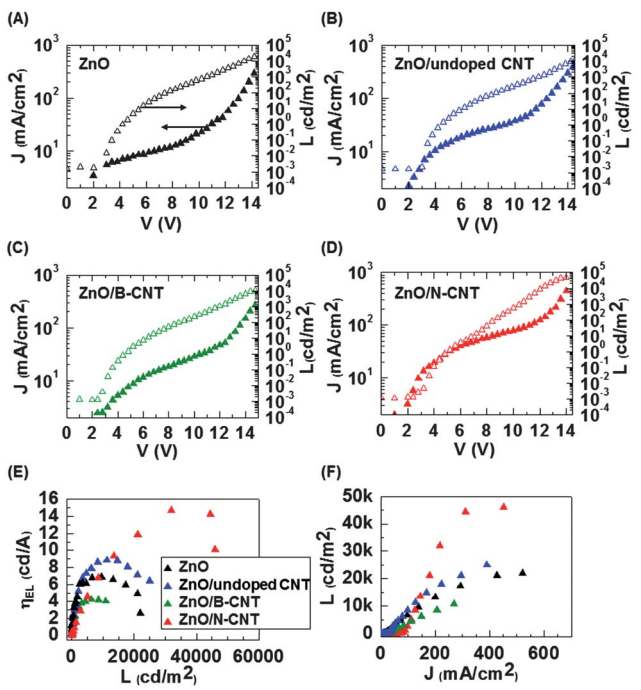

Fig. 4 *J*–*V*–*L* characteristics of OLEDs (A) without CNTs, (B) with undoped CNTs, (C) with B-CNTs, and (D) with N-CNTs in the ZnO electron transport layer. (E) η_{EL}–*L* and (F) *L*–*J* curves for ZnO electron transport layers with various CNTs.

Table 1 Summary of light-emitting characteristics of OLEDs with ZnO electron transport layers incorporated with undoped CNT, B-CNT or N-CNT, and a 400 nm thick light-emitting F8BT layer. The FTO cathode and the MoO_3 deposited Au anode were commonly used for all devices

Device configuration	L_{max} (cd m^{-2}) (@ bias)	η_{max} (cd A^{-1}) (@ bias)	η_{max} (lm W^{-1}) (@ bias)	EQE_{max} (%) (@ bias)
ZnO	21 000 (@ 14.6 V)	6.9 (@ 13.4 V)	1.6 (@ 13.0 V)	2.2 (@ 13.4 V)
ZnO/undoped CNT (0.08 wt%)	25 000 (@ 14.4 V)	8.9 (@ 12.8 V)	2.2 (@ 12.4 V)	2.8 (@ 12.8 V)
ZnO/B-CNT (0.08 wt%)	10 900 (@ 14.8 V)	4.2 (@ 14.0 V)	0.9 (@ 14.0 V)	1.3 (@ 14.0 V)
ZnO/N-CNT (0.08 wt%)	46 100 (@ 14.0 V)	14.3 (@ 13.6 V)	3.5 (@ 13.2 V)	4.3 (@ 13.2 V)

(compare *J–V* plots in Fig. 4), a weak electron dominant behavior was observed although its physical origin is still unclear. The detailed device characteristics are summarized in Table 1.

The electron and hole transport within the OLEDs with pure ZnO and nanocomposite transport layers were quantitatively compared by the *J–V* characteristics of the electron-only and hole-only devices (Fig. 5). The electron-only devices were prepared as shown in an inset of Fig. 5(A). Due to the large hole injection barrier at the Ca/Al anode, electrons were dominant carriers in this modified device architecture. Without hole injection, the electron-only devices did not show any noticeable electroluminescence. As shown in Fig. 5(A), the devices with ZnO/CNT nanocomposite layers reached an electron injection current density of 0.35 mA cm^{-2} at 4.5 V for N-CNTs, at 8.0 V for undoped CNTs, and at more than 15 V for B-CNTs, respectively. The device with a pure ZnO electron transport layer reached the same current density at 12.8 V. The electron mobility was calculated using the Mott–Gurney space-charge-limited-current (SCLC) equation:[41]

$$J = \frac{9}{8}\mu_{eff}\varepsilon_0\varepsilon_r\frac{V^2}{d^3} \quad (1)$$

where J is the current density, μ_{eff} is the effective charge carrier mobility, which includes the effect of injection efficiency[42] or traps, ε_0 is the permittivity of free-space, ε_r is the relative dielectric constant, V is the applied voltage, and d is the thickness of the active layer. The *J–V* characteristics of electron-only devices were fitted with the SCLC model shown in eqn (1) (Fig. 5(B)). By employing the literature value of the relative dielectric constant (2.9)[43] and the measured thickness of 400 nm for F8BT layer, the effective electron mobility ($\mu_{eff}^{(e)}$) was calculated to be 1.5×10^{-6} cm^2 V^{-1} s^{-1} for the device without CNT, and 4.0×10^{-6} cm^2 V^{-1} s^{-1} for the device with undoped CNTs, and 8.0×10^{-7} cm^2 V^{-1} s^{-1} for the device with B-CNTs, respectively. In contrast, the device with N-CNTs showed the highest effective mobility of 7.0×10^{-6} cm^2 V^{-1} s^{-1}, which corresponded to a five-fold improvement over the device without CNTs. Under the reasonable assumption that the bulk mobility of the F8BT layer did not change, the observed difference in $\mu_{eff}^{(e)}$ should be caused by the difference in the layers underneath the F8BT layer. The hole-only device consisting of Sn:In_2O_3 (ITO), poly(3,4-ethylene dioxythiophene):poly(styrene sulfonate) (PEDOT:PSS), F8BT, MoO_3, and Au layers was investigated for hole mobility (Fig. 5(C)). Owing to the large energy gap between the PEDOT:PSS and F8BT layers, electron transport was blocked in this architecture. Mott–Gurney SCLC fitting estimated effective hole mobility ($\mu_{eff}^{(h)}$) of 6.0×10^{-6} cm^2 V^{-1} s^{-1}. A quantitative comparison of electron and hole mobilities verified that the device with a ZnO/N-CNT nanocomposite electron transport layer had a balanced electron and hole transport (Fig. 5(D)), which was greatly advantageous for high performance optoelectronic devices.

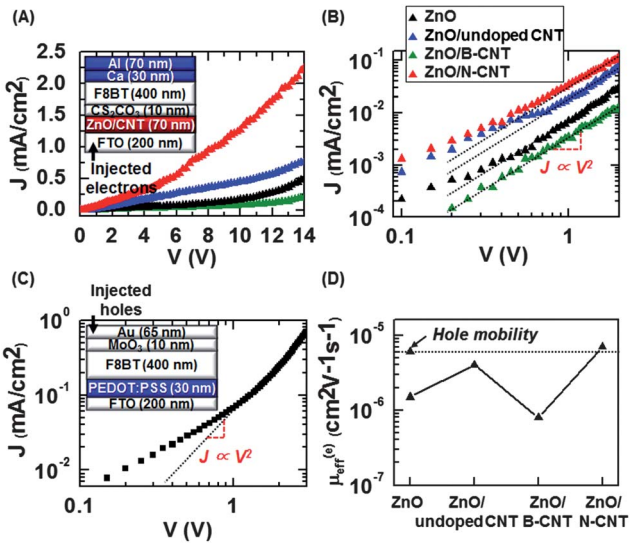

Fig. 5 (A) *J–V* characteristics (inset: an electron-only device architecture), and (B) log *J vs.* log *V* plots for Mott–Gurney SCLC fitting of the electron-only device. (C) log *J vs.* log *V* plot of *J–V* characteristics for SCLC fitting of a hole-only device. (D) Calculated electron mobilities within OLEDs with ZnO, ZnO/undoped CNT, ZnO/B-CNT, and ZnO/N-CNT electron transport layers. Each value is quantitatively obtained from the Mott–Gurney SCLC equation.

Conclusions

We have demonstrated a metal oxide/chemically doped CNT nanocomposite charge transport layer with improved charge injection and transport properties, and its successful application in high performance OLEDs. Unlike other methods to promote the electrical conductivity of metal oxides, such as foreign element doping, reinforcement with high carrier mobility nanomaterials could effectively enhance the electron mobility of metal oxides, maintaining the optical transparency, solution processability, and intrinsic bandgap energy levels. This offered an unprecedented opportunity to enhance the device performance of inverted OLEDs with minimized alteration of the device architecture and fabrication process. Additionally, due to the tunability of the CNT work function by substitutional doping, our CNT-assisted charge mobility enhancement is generally

useful for various organic and inorganic charge transport materials with different energy levels.[26,36,44,45]

Acknowledgements

The authors thank Cambridge Display Technology (CDT), Ltd., for supplying F8BT. This work was supported by the Mid-career Researcher Program (2010-0027764), the National Research Laboratory Program (R0A-2008-000-20057-0), and the World Class University (WCU) program (R32-2008-000-10051-0).

Notes and references

1 H. Ma, H.-L. Yip, F. Huang and A. K.-Y. Jen, *Adv. Funct. Mater.*, 2010, **20**, 1371.
2 R. Steim, F. R. Kogler and C. J. Brabec, *J. Mater. Chem.*, 2010, **20**, 2499.
3 N. Koch, *ChemPhysChem*, 2007, **8**, 1438.
4 Y. Shen, A. R. Hosseini, M. H. Wong and G. G. Malliaras, *ChemPhysChem*, 2004, **5**, 16.
5 Y. Cao, G. Yu, I. D. Parker and A. J. Heeger, *J. Appl. Phys.*, 2000, **88**, 3618.
6 K. Morii, T. Kawase and S. Inoue, *Appl. Phys. Lett.*, 2008, **92**, 213304.
7 P. K. H. Ho, J.-S. Kim, J. H. Burroughes, H. Becker, S. F. Y. Li, T. M. Brown, F. Cacialli and R. H. Friend, *Nature*, 2000, **404**, 481.
8 C. V. Hoven, R. Yang, A. Garcia, V. Crockettm, A. J. Heger, G. C. Bazan and T.-Q. Nguyen, *Proc. Natl. Acad. Sci. U. S. A.*, 2008, **105**, 12730.
9 A. Garcia, R. C. Bakus II, P. Zalar, C. V. Hoven, J. Z. Brzezinski and T.-Q. Nguyen, *J. Am. Chem. Soc.*, 2011, **133**, 2492.
10 H. J. Bolink, H. Brine, E. Coronado and M. Sessolo, *ACS Appl. Mater. Interfaces*, 2010, **2**, 2694.
11 H. Choi, J. S. Park, E. Jeong, G.-H. Kim, B.-R. Lee, S. O. Kim, M. H. Song, H. Y. Woo and J. Y. Kim, *Adv. Mater.*, 2011, **23**, 2759.
12 J. S. Park, B. R. Lee, E. Jeong, H.-J. Lee, J. M. Lee, J.-S. Kim, J. Y. Kim, H. Y. Woo, S. O. Kim and M. H. Song, *Appl. Phys. Lett.*, 2011, **99**, 163305.
13 J. S. Park, B. R. Lee, J. M. Lee, J.-S. Kim, S. O. Kim and M. H. Song, *Appl. Phys. Lett.*, 2010, **96**, 243306.
14 B. R. Lee, H. Choi, J. S. Park, H. J. Lee, S. O. Kim, J. Y. Kim and M. H. Song, *J. Mater. Chem.*, 2011, **21**, 2051.
15 H. J. Bolink, E. Coronado, J. Orozco and M. Sessolo, *Adv. Mater.*, 2009, **21**, 79.
16 D. Kabra, M. H. Song, B. Wenger, R. H. Friend and H. J. Snaith, *Adv. Mater.*, 2008, **20**, 3447.
17 D. Kabra, L. P. Lu, M. H. Song, H. J. Snaith and R. H. Friend, *Adv. Mater.*, 2010, **22**, 3194.
18 H. J. Bolink, E. Coronado, D. Repetto, M. Sessolo, E. M. Barea, J. Bisquert, G. Garcia-Belmonte, J. Prochazka and L. Kavan, *Adv. Funct. Mater.*, 2008, **18**, 145.
19 N. Tokmoldin, N. Griffiths, D. D. C. Bradley and S. A. Haque, *Adv. Mater.*, 2009, **21**, 3475.
20 H. J. Bolink, H. Brine, E. Coronado and M. Sessolo, *J. Mater. Chem.*, 2010, **20**, 4047.
21 M. Sessolo and H. J. Bolink, *Adv. Mater.*, 2011, **23**, 1829.
22 V. Bhosle, A. Tiwari and J. Narayan, *Appl. Phys. Lett.*, 2006, **88**, 032106.
23 J. G. Lu, Y. Z. Zhang, Z. Z. Ye, Y. J. Zeng, H. P. He, L. P. Zhu, J. Y. Huang, L. Wang, J. Yuan, B. H. Zhao and X. H. Li, *Appl. Phys. Lett.*, 2006, **89**, 112113.
24 W. J. E. Beek, M. M. Wienk, M. Kemerink, X. Yang and R. A. J. Janssen, *J. Phys. Chem. B*, 2005, **109**, 9505.
25 S. H. Lee, D. H. Lee, W. J. Lee and S. O. Kim, *Adv. Funct. Mater.*, 2011, **21**, 1338.
26 D. H. Lee, J. E. Kim, T. H. Han, J. W. Hwang, S. Jeon, S.-Y. Choi, S. H. Hong, W. J. Lee, R. S. Ruoff and S. O. Kim, *Adv. Mater.*, 2010, **22**, 1247.
27 J. O. Hwang, D. H. Lee, J. Y. Kim, T. H. Han, B. H. Kim, M. Park, K. No and S. O. Kim, *J. Mater. Chem.*, 2011, **21**, 3432.
28 D. S. Hecht, L. Hu and G. Irvin, *Adv. Mater.*, 2011, **23**, 1482.
29 S. Berson, R. de Bettignies, S. Bailly, S. Guillerez and B. Jousselme, *Adv. Funct. Mater.*, 2007, **17**, 3363.
30 S. Chaudhary, H. Lu, A. M. Müller, C. J. Bardeen and M. Ozkan, *Nano Lett.*, 2007, **7**, 1973.
31 K.-Y. Chun, S. K. Choi, H. J. Kang, C. Y. Park and C. J. Lee, *Carbon*, 2006, **44**, 1491.
32 X. Dong, D. Fu, W. Fang, Y. Shi, P. Chen and L.-J. Li, *Small*, 2009, **5**, 1422.
33 Y. Shi, K. K. Kim, A. Reina, M. Hofmann, L.-J. Li and J. Kong, *ACS Nano*, 2010, **4**, 2689.
34 D. H. Lee, W. J. Lee and S. O. Kim, *Nano Lett.*, 2009, **9**, 1427.
35 D. H. Lee, W. J. Lee, W. J. Lee, S. O. Kim and Y.-H. Kim, *Phys. Rev. Lett.*, 2011, **106**, 175502.
36 J. M. Lee, J. S. Park, S. H. Lee, H. Kim, S. Yoo and S. O. Kim, *Adv. Mater.*, 2011, **23**, 629.
37 Y. Nakayama, K. Morii, Y. Suzuki, H. Machida, S. Kera, N. Ueno, H. Kitagawa, Y. Noguchi and H. Ishii, *Adv. Funct. Mater.*, 2009, **19**, 3746.
38 M. Kroger, S. Hamwi, J. Meyer, T. Riedl, W. Kowalsky and A. Kahn, *Appl. Phys. Lett.*, 2009, **95**, 123301.
39 X. M. Liu, H. E. Romero, H. R. Gutierrez and P. C. Eklund, *Nano Lett.*, 2008, **8**, 2613.
40 E. Borowiak-Palen, T. Pichler, A. Graff, R. J. Kalenczuk, M. Knupfer and J. Fink, *Carbon*, 2004, **42**, 1123.
41 P. W. M. Blom, M. J. M. de Jong and M. G. van Munster, *Phys. Rev. B: Condens. Matter*, 1997, **55**, R656.
42 Y. Shen, D. B. Jacobs, G. G. Malliaras, G. Koley, M. G. Spencer and A. Ioannidis, *Adv. Mater.*, 2001, **13**, 1234.
43 M. Schidleja, C. Melzer and H. von Seggern, *Adv. Mater.*, 2009, **21**, 1172.
44 J. O. Hwang, J. S. Park, D. S. Choi, J. Y. Kim, S. H. Lee, K. E. Lee, Y.-H. Kim, M. H. Song, S. Yoo and S. O. Kim, *ACS Nano*, 2012, **6**, 159.
45 S. Park, Y. Hu, J. O. Hwang, E.-S. Lee, L. B. Casabianca, W. Cai, J. R. Potts, H.-W. Ha, S. Chen, J. H. Oh, S. O. Kim, Y.-H. Kim, Y. Ishii and R. S. Ruoff, *Nat. Commun.*, 2012, **3**, 638.

